



LAWRENCE  
LIVERMORE  
NATIONAL  
LABORATORY

# Absolute calibration of the continuum x-ray spectrometer (ConSpec) at the National Ignition Facility

M. J. MacDonald, B. Kozioziemski, A. G. MacPhee, M. B. Schneider, J. Ayers, D. B. Thorn

September 18, 2019

Journal of Instrumentation

## **Disclaimer**

---

This document was prepared as an account of work sponsored by an agency of the United States government. Neither the United States government nor Lawrence Livermore National Security, LLC, nor any of their employees makes any warranty, expressed or implied, or assumes any legal liability or responsibility for the accuracy, completeness, or usefulness of any information, apparatus, product, or process disclosed, or represents that its use would not infringe privately owned rights. Reference herein to any specific commercial product, process, or service by trade name, trademark, manufacturer, or otherwise does not necessarily constitute or imply its endorsement, recommendation, or favoring by the United States government or Lawrence Livermore National Security, LLC. The views and opinions of authors expressed herein do not necessarily state or reflect those of the United States government or Lawrence Livermore National Security, LLC, and shall not be used for advertising or product endorsement purposes.

# Absolute calibration of the continuum x-ray spectrometer (ConSpec) at the National Ignition Facility

---

**M. J. MacDonald, B. Koziowski, A. G. MacPhee, M. B. Schneider, J. Ayers, and D. B. Thorn**

*Lawrence Livermore National Laboratory, Livermore, California 94550*

*E-mail:* [macdonald10@llnl.gov](mailto:macdonald10@llnl.gov)

**ABSTRACT:** We present the absolute calibration of the continuum x-ray spectrometer (ConSpec), designed to measure the hot-spot electron temperature of inertial confinement fusion (ICF) implosions at the National Ignition Facility (NIF). The spectrometer measures emission from photon energies of 20 to 30 keV where opacity effects in ICF implosions at the NIF are negligible and provides spatial resolution to separate the hot-spot emission from other x-ray sources, such as the gold emission from the hohlraum wall. Using a combination of x-ray ray tracing and calibration data taken using a well characterized x-ray source, we measure the dispersion, spatial resolution, and absolute sensitivity of the instrument. Finally, we present an example spectrum measured at the NIF and demonstrate the ability to measure the hot-spot electron temperature with uncertainty under 10%.

**KEYWORDS:** Spectrometers, Plasma diagnostics - interferometry, spectroscopy and imaging

---

<sup>1</sup>Corresponding author

<sup>2</sup>LLNL-JRNL-790347-DRAFT

---

## Contents

<b>1</b>	<b>Introduction</b>	<b>1</b>
<b>2</b>	<b>X-ray continuum emission</b>	<b>2</b>
<b>3</b>	<b>ConSpec design</b>	<b>2</b>
<b>4</b>	<b>X-ray calibration measurements</b>	<b>5</b>
4.1	Measured dispersion	5
4.2	Spatial resolution	6
4.3	Sensitivity and flat fielding analysis	7
4.4	X-ray calibration source analysis	9
4.5	Example result from the National Ignition Facility	10
<b>5</b>	<b>Conclusions</b>	<b>12</b>

---

## 1 Introduction

The temperature and density of the hot-spot created in inertial confinement fusion (ICF) implosions is a key metric for the implosion performance. Accurate measurements of these quantities are required to constrain theoretical models of ICF implosions and assess implosion performance using simulation tools. Ion temperature ( $T_i$ ) is typically inferred from the velocity distribution measured in the neutron spectra created from the DT and DD fusion reactions, measured by nuclear time-of-flight (nTOF) diagnostics, however these measurements are affected by residual kinetic energy in the form of turbulence and bulk fluid velocity flows in the hot-spot. Due to the extremely high thermal velocity of electrons, which is many times higher than the velocity of bulk flows in the plasma, the electron temperature ( $T_e$ ) is not sensitive to residual kinetic energy effects that affect  $T_i$  measurements, necessitating the development of reliable  $T_e$  diagnostics at the National Ignition Facility (NIF).

In order to mitigate x-ray opacity effects,  $T_e$  measurements at the NIF are most reliable at photon energies above approximately 15 keV. At lower photon energies the opacity of the remaining fuel layer and ablator material at densities on the order of 100 g/cc introduce significant uncertainties in the analysis of x-ray emission spectra, especially at high convergence where hydrodynamic instabilities create significant variations in the shell thickness. At photon energies above 20 keV, opacity effects are negligible. Currently at the NIF, the standard  $T_e$  diagnostic uses a set of titanium filters of varying thickness to infer the slope of the hard x-ray continuum [1, 2]. Although this method has been successful in providing a time-integrated  $T_e$  for ICF implosions, the analysis assumes a known x-ray emission spectrum and the combination of low signal level through the

thicker filters and the non-collecting geometry of the diagnostic limits the technique to time-integrated measurements.

In order to address these two concerns, we have developed the continuum x-ray spectrometer (ConSpec) at the NIF [3]. The ConSpec uses a conically curved crystal to measure x-ray emission spectra from 20 to 30 keV. The conical crystal optic in the Hall geometry [4] produces a line focus at the detector plane, providing high signal levels suitable for future time-resolved x-ray continuum measurements. The Hall geometry is particularly useful at large scale laser facilities, where the detector plane is perpendicular to the diagnostic axis when using electronic detectors (e.g. x-ray framing cameras or streak cameras).

## 2 X-ray continuum emission

The hard x-ray continuum from an ICF hot-spot consists of two components: free-free emission created by free electrons scattering off ions in the plasma and free-bound emission resulting from free electrons falling into bound states of the ions. The free-free emissivity for a fully ionized species is given by [5]

$$\epsilon_{\nu}^{FF} = \frac{32}{3} \sqrt{\frac{\pi}{3}} \alpha^3 \chi_H a_0^3 n_e n_i \langle Z^2 g_{FF} \rangle \left( \frac{\chi_H}{kT_e} \right)^{1/2} e^{-h\nu/kT_e}, \quad (2.1)$$

where  $k$  is the Boltzmann constant,  $\alpha$  is the fine structure constant,  $a_0$  is the Bohr radius,  $\chi_H$  is the ionization energy of hydrogen,  $g_{FF}$  is the Gaunt factor for free-free emission [7], and  $Z$  is the ion charge ( $\langle Z^2 \rangle = \sum_i Z_i^2$  for a mixture of ion species). The free-bound emissivity for a given component is given by

$$\epsilon_{\nu}^{FB} = \frac{64}{3} \sqrt{\frac{\pi}{3}} \alpha^3 \chi_H a_0^3 n_e n_i \langle Z^4 e^{(\chi - \Delta\chi)/kT} g_{FB} \rangle \left( \frac{\chi_H}{kT_e} \right)^{3/2} e^{-h\nu/kT_e}, \quad (2.2)$$

where  $\chi$  is the ionization energy of the H-like ion of the species,  $\Delta\chi$  is an ionization energy correction for continuum lowering [6], and  $g_{FB}$  is the free-bound Gaunt factor.

For hydrogen isotopes deuterium (D) and tritium (T), the free-bound contribution is negligible and we only need to consider the free-free emission. For higher  $Z$  elements, the free-bound contribution can become significant. The "excess" continuum from free-bound emission has been used to estimate the amount of carbon from the ablator mixed into the hot-spot at the NIF [8] and at OMEGA laser facility [5]. The  $Z^4$  scaling of the free-bound emissivity makes it very important to include in spectral calculations if the plasma contains multiple elements. For example, for a mixture of DD with 0.01% Kr at  $T_e = 3.7$  keV and  $n_e = 1 \times 10^{24} \text{ cm}^{-3}$ , the free-bound emissivity from the Kr is approximately two times brighter than the total free-free emissivity.

## 3 ConSpec design

The NIF continuum x-ray spectrometer (ConSpec) uses a conically curved highly annealed pyrolytic graphite crystal (HAPG) to measure 20–30 keV x-rays. The instrument is currently configured to operate in the 90-78 (chamber coordinates  $\theta = 90^\circ$ ,  $\phi = 78^\circ$ ) Diagnostic Manipulator (DIM) at the NIF. The instrument consists of several components, shown schematically in Figure 1b: the conical

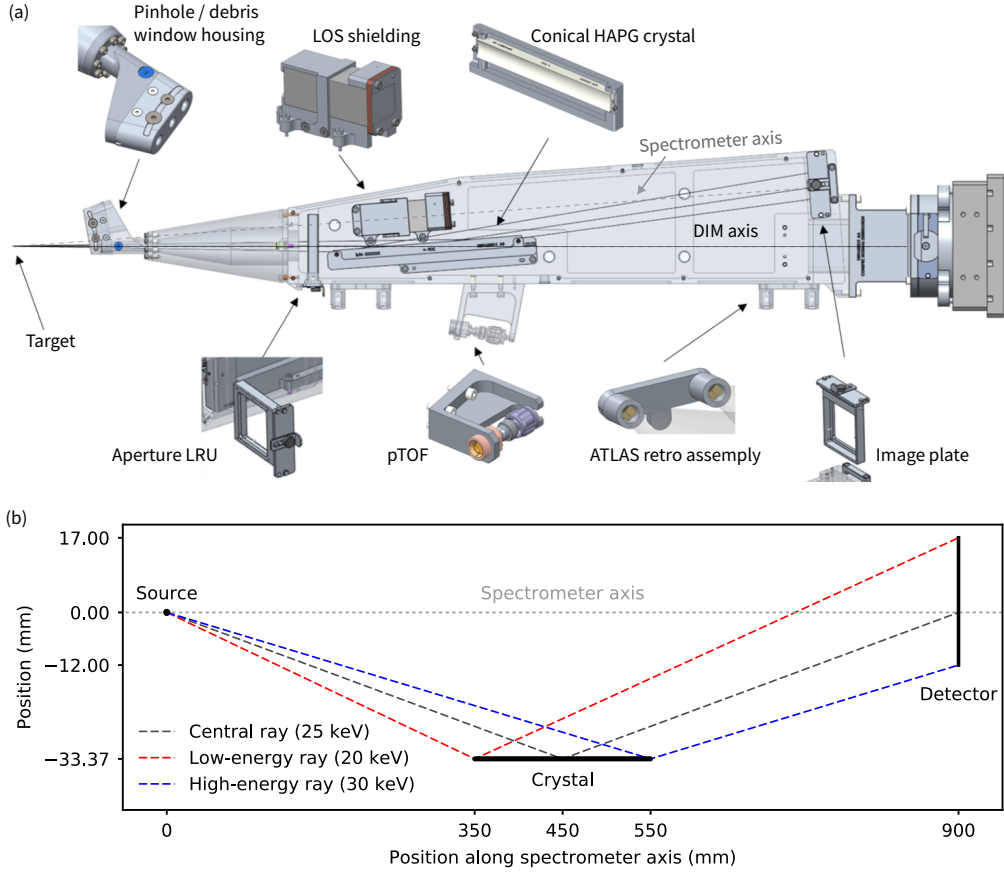


**Figure 1.** (a) Drawing showing the layout of the ConSpec components. The DIM axis is shown in black and the spectrometer is shown in gray (the axis from the target to the center ray on the detector). The spectrometer axis is rotated  $4.24^\circ$  from the DIM axis. (b) Ray tracing setup showing the position and orientation of the crystal and detector relative to the spectrometer axis.

HAPG crystal optic, an aperture to limit the active area of the crystal, and an image plate holder. The instrument also includes pinholes for the x-ray penumbral imaging using ARIANE [9, 10] in 90-89 and the Dilation X-ray Imager (DIXI) [11–13] in 90-100, as well as a particle time of flight (PTOF) detector. The ConSpec records time-integrated spectra on image plate, however the design could be easily modified to be coupled to an x-ray streak camera in the future for time-resolved  $T_e$  measurements. The detailed design of the diagnostic have been published by Thorn *et al.* [3].

The HAPG crystal, procured from Optigraph, is  $25\text{-}\mu\text{m}$ -thick with an estimated mosaic spread of  $0.15^\circ$  on a diamond-turned aluminum substrate. HAPG was chosen for its excellent reflectivity and ability to be used in strongly bent geometries [14]. The dimensions of the crystal are 200 mm in the dispersion (meridional) direction and 25 mm in the imaging (sagittal) direction, with the center at 450 mm from target chamber center (TCC). The radius of curvature varies along the length of the conical crystal surface, decreasing from 40 mm at 20 keV to 25 mm at 30 keV. The diffracted x-rays are recorded on an image plate placed 900 mm from TCC. A schematic of the ray tracing setup with the relevant dimensions is shown in Figure 1b. The substrate metrology showed that the

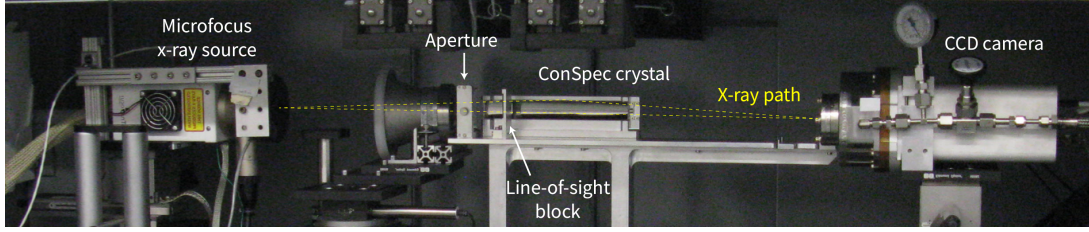


**Figure 2.** Calibration setup using a microfocus x-ray source to collect spectra on multiple detectors.

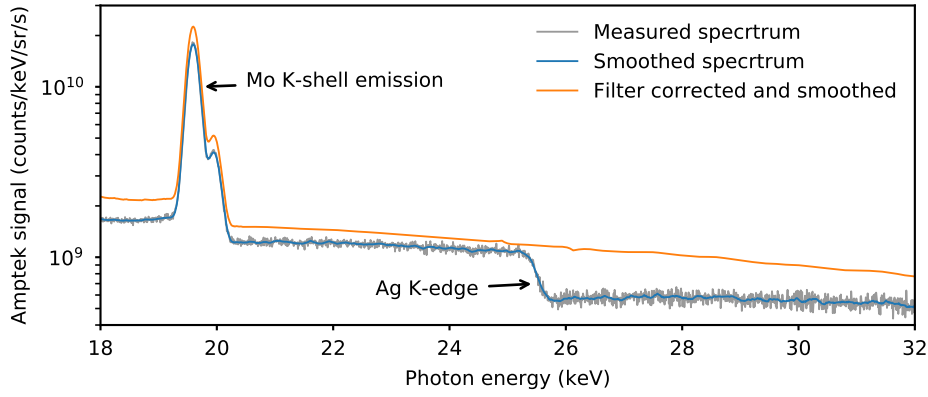


**Figure 3.** Source spectrum,  $S(h\nu)$ , measured using the Amptek SDD with a  $408 \mu\text{m}$  diameter pinhole and a  $12.5 \mu\text{m}$  Ag filter (gray), smoothed (blue), and smoothed and filter corrected (orange) in units of counts/s/sr for the x-ray source operated at 65 kV and 0.075 mA with a Mo anode. The Mo K-shell emission lines and the Ag K-edge were used to calibrate the energy axis of the Amptek data.

root-mean-square deviation of the surface is under  $90 \text{ \AA}$ . The aperture placed in front of the crystal is available in 0.5, 1, 2, 5, and 10 mm widths to limit the active area of the crystal to adjust the flux detected by the IP.

The conical crystal uses the Hall geometry, where the half-angle of the cone is equal to the Bragg angle at the central energy of the spectrometer. The opening angle of the ConSpec crystal is  $4.24^\circ$ , corresponding to the Bragg angle for 25 keV using HAPG. The Hall geometry produces a line focus perpendicular to the spectrometer axis, allowing the spectra to be recorded by DIM-based detectors at the NIF. The conical geometry provides sufficient spatial resolution to allow the hot-spot emission to be separated from the emission from the hohlraum walls directly irradiated by the laser. Without the spatial resolution of the diagnostic, the bright emission from the hohlraum walls would contaminate the hot-spot emission, preventing a useful measurement of the hot-spot conditions. Due to the large length of the crystal, the magnification of the system varies significantly over the spectral range. The magnification is 1.00 at the central x-ray energy of 25 keV, 1.57 at 20 keV, and 0.64 at 30 keV.

## 4 X-ray calibration measurements

X-ray calibration measurements were made at the NIF x-ray optic calibration facility at LLNL using a Truefocus TFX-8100 microfocus x-ray source with a Mo anode. The setup of the calibration measurements is shown in Figure 2, showing the x-ray source on the left, the ConSpec crystal and slit aperture in the center, and the detector on the right. Alignment and characterization of the system was performed using a CCD camera (as shown in Figure 2) and calibration measurements were made using Fuji Biological Analysis System (BAS) SR-type image plate and an Amptek XR-100SDD Silicon Drift Detector (SDD). The Amptek SDD is a photon counting x-ray spectrometer with a quantum efficiency of 15–40% and spectral resolution of  $\approx 250$  eV full width at half maximum (FWHM) over the range of 20–30 keV.

The ConSpec was placed on a calibration fixture designed to replicate the geometry on the NIF, with the crystal optic parallel to the axis of the instrument as shown in Figure 1b. A pair of tungsten-wire crosshairs on the calibration fixture defined the instrument axis. The instrument axis was made co-linear with the x-ray axis by adjustment of relative positions of the instrument and x-ray system until the shadows of the two crosshairs overlapped on the CCD. A mechanical fixture allowed the CCD to be removed, and the image plate to be placed in the same location. The portable coordinate measurement machine (Faro Prime) was used to set the distance between the x-ray source and the ConSpec crystal. The fabrication tolerances and measurement uncertainties allow alignment of the system to within  $500 \mu\text{m}$  of the as-built NIF configuration.

The x-ray source was operated at an electron accelerating voltage of 65 kV onto a Mo anode to provide sufficient x-ray emission at photon energies of 20–30 keV. The microfocus source has a  $15 \mu\text{m}$  source size, which is much smaller than the spatial resolution of the ConSpec and can be treated as a point source. The source spectrum,  $S(h\nu)$ , was measured by placing the Amptek SDD 855.1 mm from the x-ray source and installing a Ta substrate with a pinhole with a  $408 \mu\text{m}$  diameter over the diode, corresponding to a solid angle of  $1.79 \times 10^{-7}$  sr. The thickness of the Ta pinhole substrate was  $2000 \mu\text{m}$  to sufficiently attenuate all emission below the 65 keV cutoff of the x-ray source and a  $12.5\text{-}\mu\text{m}$ -thick Ag filter was used in the source measurements to provide a fiducial for energy calibration. Figure 3 shows the measured x-ray source spectrum measured by the Amptek detector in units of counts/keV/s/sr showing the Mo K-shell emission around 19 keV and the Ag K-edge at 25.5 keV, which were used to calibrate the energy axis of the measured spectrum. The raw data (gray) was smoothed using a Savitzky-Golay filter using third-order polynomials and a window size of 31.

### 4.1 Measured dispersion

The dispersion of the instrument was measured using spectral lines and filter absorption edges recorded on Fuji BAS-SR image plate. Figure 4a shows the image plate data with the Mo K- $\beta$  emission lines from the anode (19.59, 19.61, 19.97 keV) and two absorption edges from the filters: Ag at 25.51 keV and Sn at 29.20 keV.

The spatial lineout of the image plate data is shown in Figure 4b, with the emission lines and absorption features labeled. The theoretical dispersion from ray tracing analysis along with the measured feature locations and best fit to the data are shown in Figure 4c. The slight difference between the fit to the calibration data and the theoretical dispersion from ray tracing is due to slight

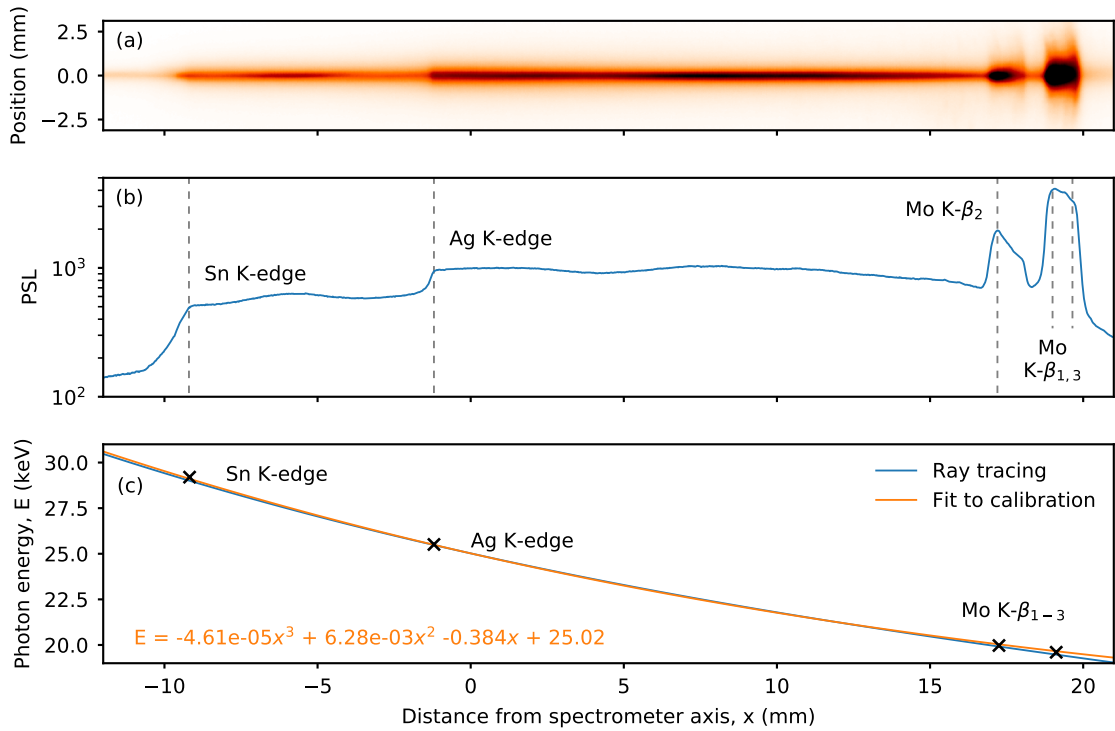


**Figure 4.** (a) Image plate data from the x-ray calibration station using a 5 mm aperture, exposed for one hour exposure using a Mo anode operated at 65 kV and 0.075 mA with Ag and Sn filters. (b) Spectrally-resolved line out with dashed lines marking the characteristic lines from the anode and the absorption edges of the filters. (c) ConSpec dispersion calculated from x-ray ray tracing (blue) and a cubic fit (orange) to the calibration data (black crosses).

differences between the nominal ConSpec design and the as-built instrument. The best fit to the image plate data dispersion is  $E = (-4.61 \times 10^{-5})x^3 + (6.28 \times 10^{-3})x^2 - 0.384x + 25.02$ , where  $E$  is the photon energy in keV and  $x$  is the position from the spectrometer axis in mm.

## 4.2 Spatial resolution

The image plate data was used to measure the spatial resolution of the diagnostic for 1, 5, and 10 mm apertures over the full spectral range of the detector by calculating the point spread function of the 15  $\mu\text{m}$  microfocus x-ray source. Figure 5a shows a lineout of the image plate data at 24 keV with the 5 mm aperture with a Voigt function fit to the measurement. The spatial resolution is taken to be the FWHM of the Voigt fit, which for the lineout shown is 550  $\mu\text{m}$ .

Figure 5b shows the measured spatial resolution for each aperture width measured across the entire spectral range of the instrument. The 1 and 5 mm apertures have nearly identical spatial resolution, while the 10 mm aperture begins to degrade the spatial resolution due to larger focussing errors created by using a larger active area of the conical crystal. The sharp changes in spatial resolution at the Ag and Sn filter absorption edges (25.5 and 29.2 keV) can be attributed to the imperfect imaging of the conical crystal geometry, which does not produce a perfect line focus. The focussing errors distribute a small amount of the signal from a given photon energy into the

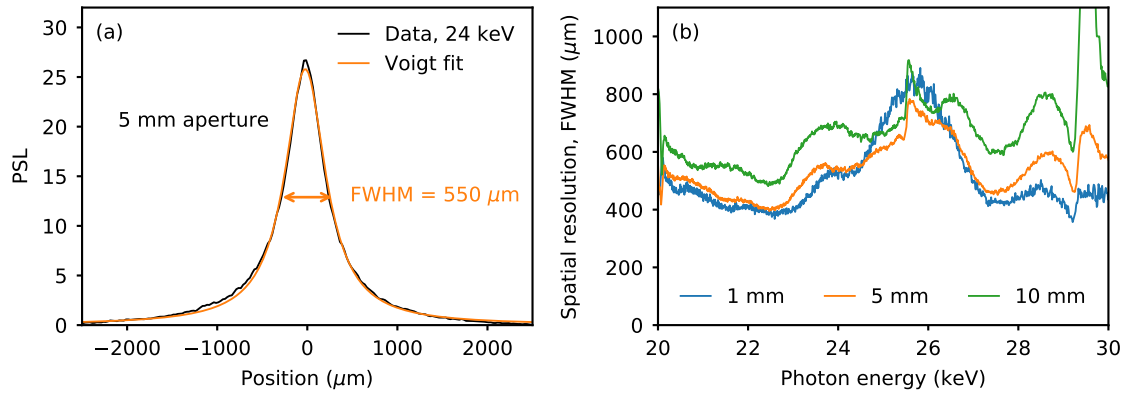


**Figure 5.** (a) Lineout of the image plate calibration data taken at 24 keV for the 5 mm aperture and the Voigt fit and (b) spatial resolution measurements using 1, 5, and 10 mm apertures over the full spectral range of the diagnostic.

wings of the focus, with the proportion of signal in the wings increasing with aperture size (see Martinolli *et al.* [15]). The positions just above the filter edges contain a reduced signal from the nominal photon energy along the focal line (due to the absorption edge) and the unattenuated wings from photon energies just below the absorption edge, resulting in an increase in the FWHM of the fit to the lineout. As expected, this effect increases with aperture width due to an increasing proportion of signal in the wings. This effect only occurs for absorption edges and would not affect measurements using line emission.

### 4.3 Sensitivity and flat fielding analysis

The absolute sensitivity of the crystal as a function of photon energy,  $G(h\nu)$ , is given by [16]

$$G(h\nu) = \frac{d\Omega}{dA} \frac{dh\nu}{d\theta_B} R(h\nu) \quad (4.1)$$

where  $\Omega$  is the solid angle of the active area of the crystal,  $A$  is the area on the detector plane,  $\theta_B$  is the Bragg angle, and  $R(h\nu)$  is the integrated reflectivity of the crystal. The  $d\Omega/dA$  term accounts for the focussing properties of the crystal, increasing as a larger solid angle of the crystal maps to a smaller area on the detector plane. The  $dh\nu/d\theta_B$  term is the derivative of Bragg's law, accounting for how rapidly the diffracted photon energy changes along the surface of the crystal. The units of  $G(h\nu)$  are in photon energy per unit solid angle per area on the detector (e.g. eV sr/mm<sup>2</sup>). Thus, a source spectrum,  $S(h\nu)$ , expressed in energy per unit bandwidth per unit solid angle (e.g. J/eV/sr) to be converted to measured energy deposited on the detector per unit area (e.g. J/mm<sup>2</sup>) by  $M(h\nu) = S(h\nu)G(h\nu)$ .

The sensitivity of the ConSpec can be adjusted by changing the width of the slit aperture (changing the active area on the crystal). In order to reduce the effect of aberrations in the conical focussing geometry, the slit size should be minimized while maintaining adequate signal levels for a given experiment. For the ConSpec, slit apertures larger than 10 mm introduce significant aberrations (reducing both spatial and spectral resolution), while for apertures of 5 mm and below the resolution is limited by the focussing characteristics of the optic (as seen in Figure 5).

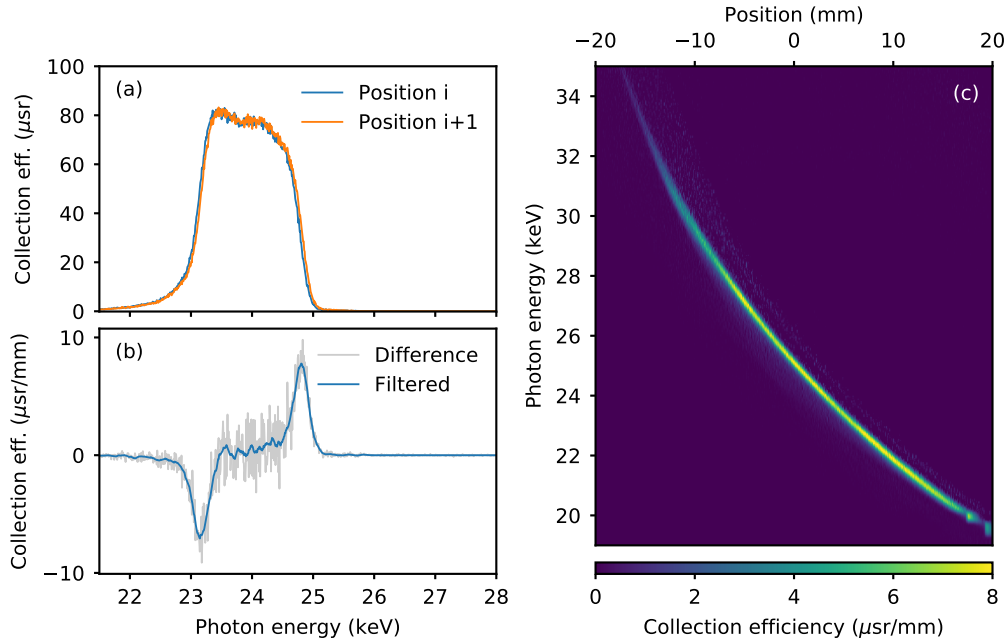


**Figure 6.** Results of scanning the Amptek SDD along the ConSpec focus using its full collection area of  $17 \text{ mm}^2$  in  $100 \mu\text{m}$  steps. (a) Spectra collected at two adjacent positions of the scan and (b) the difference of the spectra, showing the change in the spectrum measured after the move. (c) The difference spectrum for each position along the focus, showing the spectral range detected at each position with  $100 \mu\text{m}$  resolution.

The absolute sensitivity of the ConSpec was calculated by dividing the spectrum at the detector plane by the x-ray source spectrum, both of which were measured using the Amptek SDD. By measuring both the source and collected spectrum using the same instrument, we measure the fractional throughput and the results do not depend on the absolute quantum efficiency calibration of the detector.

To measure the x-ray spectrum at each point along the detector plane, we scanned the Amptek SDD along the focal line of the spectrometer with no aperture (using the full collection area of the detector of  $17 \text{ mm}^2$ ), collecting spectra at  $100 \mu\text{m}$  steps. Examples of collection efficiency spectra in from two adjacent positions are shown in Figure 6a, calculated by dividing the spectrum measured by the Amptek SDD at each position (counts/keV/s) by the source spectrum (counts/keV/sr/s).

Figure 6b shows the difference between the two scans, where the increase in signal around 24.8 keV corresponds to the additional signal in the  $100 \mu\text{m}$  space covered by the detector after the move and the decrease around 23.1 keV corresponds to the emission spectrum not captured at the new position. The raw data (gray) was smoothed using a Savitzky-Golay filter using third-order polynomials and a window size of 31. The difference spectrum is given in units of  $\mu\text{sr}/\text{mm}$  to account for the  $100 \mu\text{m}$  step size used in these measurements.

Thus, we obtain the absolute collection efficiency of the spectrometer as a function of both position (along the focal line) and photon energy, as shown in Figure 6c. To improve the signal-to-noise of the difference data, both the positive and negative peaks from Figure 6b were included in the collection efficiency calculation, where the spatial offset of the two peaks was taken into account

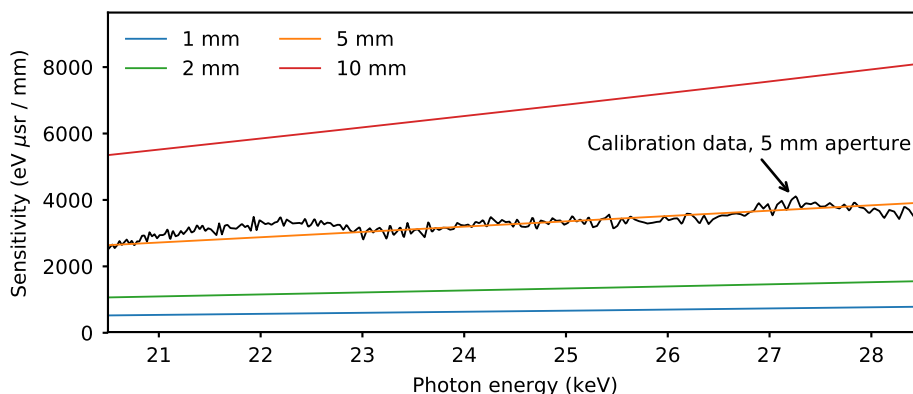


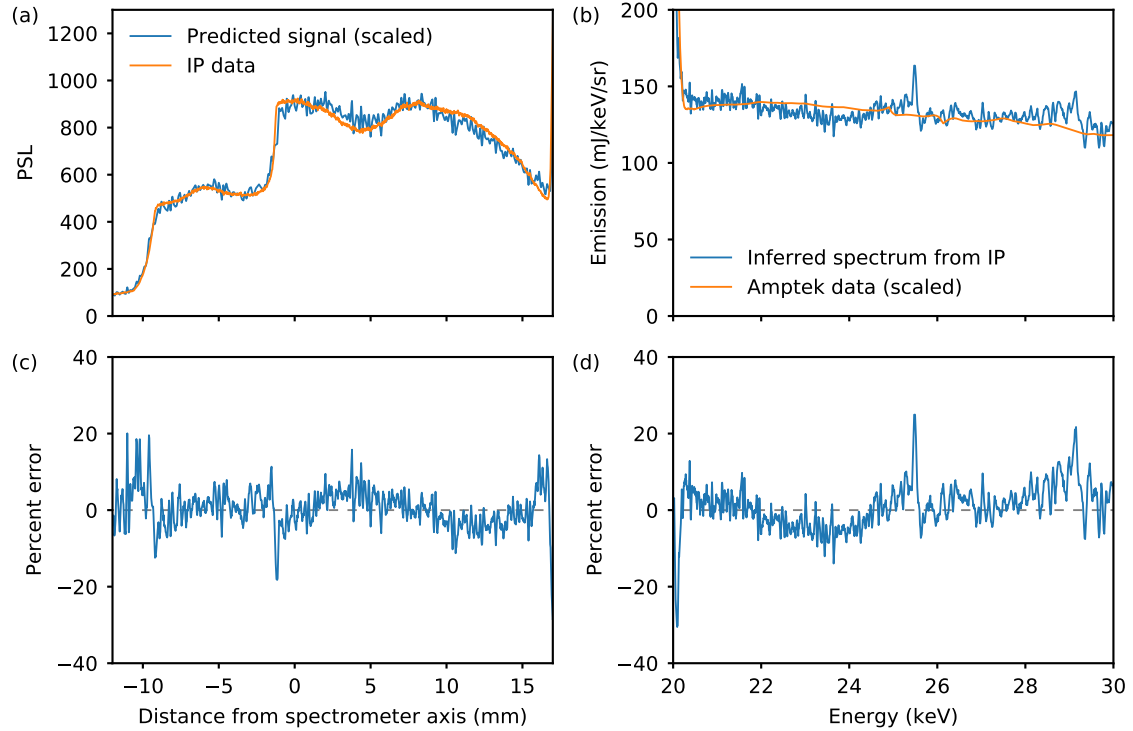
**Figure 7.** Measured ConSpec sensitivity using a 5 mm aperture compared to calculations for 1, 2, 5, and 10 mm aperture widths using ray tracing and XOP to calculate the integrated reflectivity of crystal. The minor deviations in the measured data are due to imperfections in the crystal, which are removed by using the sensitivity data in Figure 6c to flat field measured spectra.

(opposite edges of the Amptek diode) and the absolute value of two signals were averaged.

The spectrometer sensitivity can be calculated directly from the collection efficiency data by summing along the energy axis of Figure 6c, yielding  $G(x)$  in units of  $\text{keV} \cdot \mu\text{sr}/\text{mm}$ . The theoretical integrated reflectivity,  $R(h\nu)$ , of the  $25 \mu\text{m}$  HAPG crystal with  $0.15^\circ$  mosaic spread was calculated using the XCRYSTAL package in XOP for the (002) plane of HAPG [17]. Using the measured spectrometer dispersion, we convert  $G(x)$  to  $G(h\nu)$  and compare the measurement to the sensitivity calculated from ray tracing analysis, the integrated reflectivity from XOP, and Eq. 4.1. Figure 7 shows the calibration results using a 5 mm aperture compared to sensitivities calculated for various aperture widths. In order to match the calibration data, the integrated reflectivity of the crystal calculated using XOP had to be increased slightly by increasing the crystal thickness to  $32 \mu\text{m}$  while keeping the mosaic spread of the HAPG crystal at  $0.15^\circ$ . This minor difference is likely due to the fact that the ray tracing model used in this work does not explicitly include the mosaicity of the crystal except for the integrated crystal reflectivity from XOP. This corrected reflectivity was applied to all ray tracing calculations to accurately model the response of the diagnostic for each aperture width.

#### 4.4 X-ray calibration source analysis

To test the calibration of the ConSpec we performed two tests to model the calibration x-ray source using the Amptek SDD and data taken using image plate at the detector plane. First, we performed a forward fit to the image plate data using the measured source spectrum, as shown in Figure 8a. To do this, the collection efficiency data (Figure 6c) is multiplied by the source spectrum ( $\text{counts}/\text{keV}/\text{sr}/\text{s}$ ) and the filter transmission is applied before integrating over the energy axis to produce a signal in  $\text{counts}/\text{mm}/\text{s}$ , which can be converted to units of photostimulated luminescence (PSL) using image plate calibration data and the quantum efficiency of the Amptek SDD. The orange line shows the measured image plate data in units of PSL and the blue line is the predicted line out using the ConSpec calibration including filter transmission. The predicted signal level was normalized to the



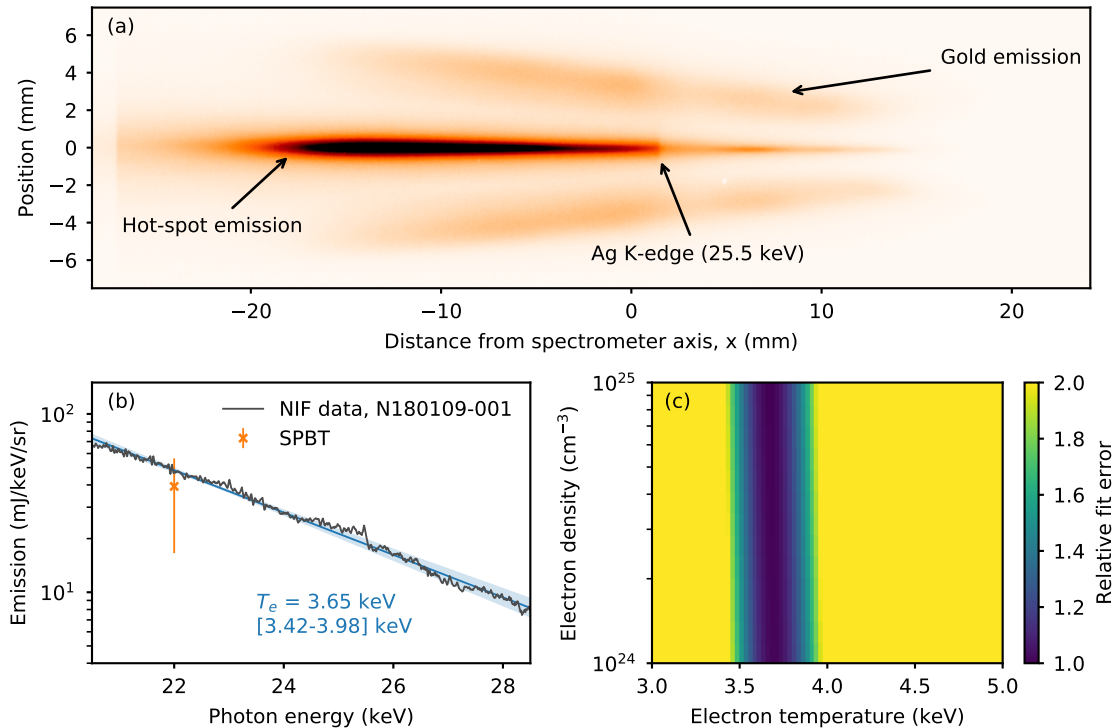
**Figure 8.** Calibration verification using the measured source spectrum and image plate data. (a) Comparison of the image plate data in orange and predicted signal for the known source in blue with corresponding error (c). (b) Comparison of the measured source spectrum in orange and the inferred spectrum in blue with corresponding error (d).

image plate data because the absolute quantum efficiency of the Amptek SDD is not well calibrated. Figure 8c shows the corresponding error in this forward fitting technique, where the error is within  $\pm 10\%$  over the range of interest.

Next, we performed the reverse process by inferring the source spectrum from the image plate data using the sensitivity curve shown in Figure 7. Figure 8b shows the measured Amptek source spectrum in orange and the inferred spectrum from the image plate in blue, where the Amptek source was again normalized to match the image plate data. The corresponding error is shown in Figure 8d, which is within  $\pm 10\%$  over the spectral range of the instrument with the exceptions of small spikes in error around the Ag and Sn filter edges. Measuring absolute emission of ICF hot-spots implosions with this accuracy is a significant improvement in the diagnostic capabilities at the NIF and will be a valuable tool to better constrain models used to assess implosion performance.

#### 4.5 Example result from the National Ignition Facility

The ConSpec has been fielded at the NIF for several implosions to measure the hot-spot electron temperature. Figure 9 shows an example spectrum from shot N180109-001, which was a symcap implosion using the BigFoot platform [18], Au hohlraum, 844- $\mu\text{m}$ -diameter W-doped HDC ablator, 3.93 mg/cm<sup>3</sup> DD gas fill with 0.01% Kr at 80K, driven with 1.1 MJ total laser energy.



**Figure 9.** (a) Image plate data from NIF shot N180109-001, showing the hot-spot emission in the center and the gold emission above and below. (b) Inferred hot-spot emission spectrum (gray) and the fit to the data using Cretin to accurately model the continuum emission from the deuterium and krypton (blue). (c) Relative fit error over the range of relevant  $T_e$  and  $n_e$  for the hot-spot showing the best fit at  $T_e = 3.65$  keV with error bounds of 3.42–3.98 keV, corresponding to  $< 10\%$  error in  $T_e$ .

The raw ConSpec data, recorded on BAS-SR image plate, is shown in Figure 9a. The bright hot-spot emission is in the center and the gold emission (from where the laser hits the hohlraum wall) is above and below and the Ag K-edge is clearly visible in the raw data, providing a spectral fiducial for calibration. The change in separation between the hot-spot and gold emission is due to the changing magnification of the instrument, which is 1 at 25 keV and decreases at higher photon energies. At high photon energies, the hot-spot and gold emission begin to overlap, limiting the useful spectral range of the time-integrated measurement to  $h\nu < 28.5$  keV. The calibrated x-ray emission spectrum recorded by ConSpec is shown in Figure 9b along with the best fit to spectral calculations using Cretin [19] and the emission measurement at 22 keV provided by the South Pole Bang Time (SPBT) diagnostic [20].

Cretin simulations were performed in 0D a for DD + 0.01% Kr plasma at  $T_e = 3 - 5$  keV and  $n_e = 10^{24} - 10^{25}$  cm<sup>-3</sup> to cover the range of expected plasma conditions for the hot-spot and normalized to match the absolute emission measured by ConSpec. The fit for each condition tested is shown in Figure 9c, showing the relative fit error normalized to the best fit. The fit was calculated for 20.5–28.5 keV, where below 20.5 keV the emission lines from the calibration x-ray source make the sensitivity data unreliable and above 28.5 keV the gold emission contaminates the hot-spot emission spectrum. The error was calculated using least-squared analysis, normalized by

the measured value at each point to properly weight the full spectral range:  $\text{error} = \sum(d - m)^2/d$ , where  $d$  is the measured data and  $m$  is the model value. Figure 9c shows the fitting analysis over the range of tested conditions, where the uncertainty in the measurement is taken to be the bounds where the error is twice that of the best fit value, corresponding to  $T_e = 3.65^{+0.33}_{-0.23}$  keV. The fitting analysis used here does not include the absolute emission level of the hot-spot, which could be used to constrain  $n_e$  if combined with the hot-spot volume inferred from x-ray imaging measurements. The measured  $T_e$  agrees with  $T_i = 3.68 \pm 0.16$  keV inferred from the DD neutron spectra recorded using nTOFs.

## 5 Conclusions

We have absolutely calibrated the throughput of the continuum x-ray spectrometer (ConSpec) using ray tracing to model the spectrometer response and calibration measurements in the laboratory. We measured the dispersion and spatial resolution of the instrument, which ranges from 400 to 800  $\mu\text{m}$  across the spectral range of the instrument. Using a well characterized micro-focus x-ray source and an Amptek SDD, we directly measured the spectrometer sensitivity and compared the results to ray tracing calculations to determine the spectrometer throughput for a range of available aperture widths. The calibration was verified by both forward fitting the shape of the measured source spectrum to predict the image plate exposure as well as inferring the source spectrum from the image plate data. Finally, we used the calibration to show that hot-spot  $T_e$  can be measured to better than 10% at the NIF. The ConSpec provides a powerful diagnostic to measure the hot-spot  $T_e$  of ICF implosions to supplement the existing set of diagnostics available at the NIF.

Future x-ray continuum spectrometers at the NIF can build on this design by using an x-ray streak camera to measure the time-resolved  $T_e$ , which will be required to better understand ICF hot-spot dynamics. Additionally, more advanced crystal geometries [21, 22] could be used to both improve the focussing characteristics of the x-ray optic and increase the collection efficiency of the diagnostic to increase the collection of high-energy photons, where the quantum efficiency of time-resolved detectors is very low. Finally, when fielded on higher performing implosions with the full set of standard diagnostics, these measurements will allow for a direct comparison of the ion and electron pressures of the hot-spot.

## Acknowledgments

The authors would like to thank Jose Castaneda, Alex Lombard, and Mai Beach for their help in performing the x-ray calibration measurements in the NIF optics calibration facility. This work was performed under the auspices of the U.S. Department of Energy by Lawrence Livermore National Laboratory under Contract DE-AC52-07NA27344 and 18-ERD-015. This material is based upon work supported by the Department Of Energy National Nuclear Security Administration under Award Number DE NA0001944. LLNL-JRNL-790347

## References

- [1] L. C. Jarrott, B. Bachmann, T. Ma, L. R. Benedetti, F. E. Field, E. P. Hartouni et al., *Thermal Temperature Measurements of Inertial Fusion Implosions*, *Physical Review Letters* **121** (2018) 085001.
- [2] L. C. Jarrott, L. R. Benedetti, H. Chen, N. Izumi, S. F. Khan, T. Ma et al., *Hotspot electron temperature from x-ray continuum measurements on the NIF*, *Review of Scientific Instruments* **87** (2016) 11E534.
- [3] D. B. Thorn, A. MacPhee, J. Ayers, J. D. Galbraith, M. C. Hardy, N. Izumi et al., *On the design of the NIF Continuum Spectrometer*, *Proc. SPIE* **10390** (2017) 1039009.
- [4] T. A. Hall, *A focusing X-ray crystal spectrograph*, *Journal of Physics E: Scientific Instruments* **17** (1984) 110–112.
- [5] R. Epstein, V. N. Goncharov, F. J. Marshall, R. Betti, R. Nora, A. R. Christopherson et al., *X-ray continuum as a measure of pressure and fuel–shell mix in compressed isobaric hydrogen implosion cores*, *Physics of Plasmas* **22** (2015) 022707.
- [6] B. J. B. Crowley, *Continuum lowering – A new perspective*, *High Energy Density Physics* **13** (2014) 84–102.
- [7] J. A. Gaunt, *Continuous Absorption*, *Philosophical transactions of the Royal Society of London* **229** (1930) 44–47.
- [8] T. Ma, P. K. Patel, N. Izumi, P. T. Springer, M. H. Key, L. J. Atherton et al., *Onset of hydrodynamic Mix in high-velocity, highly compressed inertial confinement fusion implosions*, *Physical Review Letters* **111** (2013) 1–5.
- [9] B. Bachmann, T. Hilsabeck, J. Field, N. Masters, C. Reed, T. Pardini et al., *Resolving hot spot microstructure using x-ray penumbral imaging (invited)*, *Review of Scientific Instruments* **87** (2016) 11E201.
- [10] B. Bachmann, H. Abu-Shawareb, N. Alexander, J. Ayers, C. G. Bailey, P. Bell et al., *X-ray penumbral imaging diagnostic developments at the National Ignition Facility*, *Proc. SPIE* **10390** (2017) 103900B.
- [11] T. J. Hilsabeck, J. D. Hares, J. D. Kilkenny, P. M. Bell, A. K. L. Dymoke-Bradshaw, J. A. Koch et al., *Pulse-dilation enhanced gated optical imager with 5 ps resolution (invited)*, *Review of Scientific Instruments* **81** (2010) 10E317.
- [12] S. R. Nagel, T. J. Hilsabeck, P. M. Bell, D. K. Bradley, M. J. Ayers, M. A. Barrios et al., *Dilation x-ray imager a new/faster gated x-ray imager for the NIF*, *Review of Scientific Instruments* **83** (2012) 10E116.
- [13] S. R. Nagel, T. J. Hilsabeck, P. M. Bell, D. K. Bradley, M. J. Ayers, K. Piston et al., *Investigating high speed phenomena in laser plasma interactions using dilation x-ray imager (invited)*, *Review of Scientific Instruments* **85** (2014) 11E504.
- [14] U. Zastra, A. Woldegeorgis, E. Förster, R. Loetzsch, H. Marschner and I. Uschmann, *Characterization of strongly-bent HAPG crystals for von-Hámos x-ray spectrographs*, *Journal of Instrumentation* **8** (2013) P10006–P10006.
- [15] E. Martinolli, M. Koenig, J. M. Boudenne, E. Perelli, D. Batani and T. A. Hall, *Conical crystal spectrograph for high brightness x-ray  $K\alpha$  spectroscopy in subpicosecond laser–solid interaction*, *Rev. Sci. Instrum.* **75** (2004) 5.

- [16] R. E. Marrs, G. V. Brown, J. A. Emig and R. F. Heeter, *System for calibrating the energy-dependent response of an elliptical Bragg-crystal spectrometer*, *Review of Scientific Instruments* **85** (2014) 11D626.
- [17] M. Sanchez del Rio and R. J. Dejus, *XOP v2.4: recent developments of the x-ray optics software toolkit*, *Proc. SPIE* **8141** (2011) 814115.
- [18] D. T. Casey, C. A. Thomas, K. L. Baker, B. K. Spears, M. Hohenberger, S. F. Khan et al., *The high velocity, high adiabat, "Bigfoot" campaign and tests of indirect-drive implosion scaling*, *Physics of Plasmas* **25** (2018) 056308.
- [19] H. A. Scott, *Cretin—a radiative transfer capability for laboratory plasmas*, *Journal of Quantitative Spectroscopy and Radiative Transfer* **71** (2001) 689–701.
- [20] D. H. Edgell, D. K. Bradley, E. J. Bond, S. Burns, D. A. Callahan, J. Celeste et al., *South pole bang-time diagnostic on the National Ignition Facility (invited)*, *Review of Scientific Instruments* **83** (2012) 10E119.
- [21] M. Bitter, K. W. Hill, L. Gao, P. C. Efthimion, L. Delgado-Aparicio, S. Lazerson et al., *A multi-cone x-ray imaging Bragg crystal spectrometer*, *Review of Scientific Instruments* **87** (2016) 1–2.
- [22] M. Bitter, K. W. Hill, L. Gao, B. F. Kraus, P. C. Efthimion, L. Delgado-Aparicio et al., *A new toroidal x-ray crystal spectrometer for the diagnosis of high energy density plasmas at the National Ignition Facility*, *Review of Scientific Instruments* **89** (2018) 10F118.